ISSN 1330-3651 (Print), ISSN 1848-6339 (Online)
https://doi.org/10.17559/TV-20240909001979
Original scientific paper

A Novel Work-State Analysis Method for Modelling Photovoltaic Arrays Under Multi-Illumination Conditions

Jun-Hong ZHANG*, Ling-Yu LI, Chao-Yu ZHAI

Abstract: This paper presents a novel work-state analysis method for accurate modeling of photovoltaic (PV) arrays under complex illumination conditions. Based on a refined seven-parameter model, we develop a segmented function approach that effectively captures array behavior under various lighting environments. The proposed method divides the operating regions into multiple intervals based on illumination levels, enabling precise characterization of array output. Experimental validation using a KG200GT module demonstrates modeling accuracy within 1.5% error under diverse lighting conditions. Results show that the model successfully divides the working range of local maximum power points and predicts multiple maximum power points in series configurations and accurately captures the unified characteristics in parallel arrangements. Thus, the working characteristics of series parallel arrays were analysed. The model achieves 98.5% accuracy in predicting array performance under partial shading, offering significant improvements over traditional modeling approaches. This work provides a robust mathematical framework for optimizing PV array design and maximum power point tracking algorithms in real-world applications.

Keywords: multi-illumination environment; output characteristic; photovoltaic array; segmented function model; work-state analysis method

1 INTRODUCTION

Photovoltaic array is the energy supply unit for photovoltaic power generation system. Establishing an accurate photovoltaic array model that can reflect various environmental changes is the basis for simulation research and analysis of photovoltaic power generation system.

At present, the research on photovoltaic (PV) array modelling mainly focuses on analysing the output characteristic curve of the array. Literature [1-4] comprehensively describes the output characteristics of the array, but there is no theoretical establishment of a fixed model that reflects the output characteristics and provides forward-looking analysis and prediction. The distribution characteristics of electrical parameters of photovoltaic arrays are studied under different shading conditions [5-7]. Due to the low accuracy of the engineering model itself, the study of piecewise functions has not been refined to be related to lighting. References [8] propose a method for obtaining the output characteristic curve of a PV array through linear interpolation fitting based on the measured *I-U* data of the module. Reference [9] establishes an implicit complementarity problem model for PV arrays and proposes a *I-U* characteristic solving algorithm based on utility functions, but does not consider the output under complex lighting conditions.

Therefore, it is the basis for accurately describing output characteristics to establish mathematical models of different topological structures under various lighting environments while ensuring accuracy.

The number of shadow modules is determined by introducing theoretical calculation methods of electrical parameters. However, an approximate description of the array is used, which cannot describe the fine output of the array in special environments. Based on the PV array engineering model, the segmented model is established under local shadow conditions [10]. Four advanced modeling methods for estimating the energy generated by PV systems are analysed [11]. The new method shows a mean absolute percentage error of 1.5%. The hybrid techniques are used in real-time implementation of PV array modelling [12, 13] and various configurations are investigated for the impact of partial shading location on the output power of solar photovoltaic arrays by directly constructing array simulation models [14]. While the influence of local shadows is analyzed on the maximum power point, it fails to provide the relationship between the distribution of maximum power points and local shadows. The reconfiguration technique is used to mitigate the mismatch losses due to partial shading in large-scale solar photovoltaic systems. Furthermore, these strategies are only relevant to a specific size of PV array, making it difficult to develop a comprehensive and reliable solution that works for all array sizes [15, 16].

Uniform-illumination causes a decrease in the output power of the array, and there are multiple local extreme power values in different intervals. MPPT technology can be divided into two categories in multi-illumination environments. One is to improve existing conventional methods and accurately track the global power peak under specific conditions [17, 18]. The second is based on intelligent algorithm topology, including MPPT based on fuzzy logic, artificial neural networks, artificial bee colonies [19, 20], machine learning [21] and deep learning [22], which can predict the PV power considering partial shading conditions. Although artificial intelligence algorithms do not rely on mathematical models of photovoltaic arrays, they rely on a large amount of operational data and accumulated experience to achieve complex circuits. Additional hardware costs are required.

The output current and voltage of each module in the array are different in complex lighting environments. The current or voltage values of the circuit are different in different illumination ranges, and the array operates in different states, resulting in different *I-U* characteristic equations due to the presence of bypass diodes in series modules and blocking diodes in parallel modules. A multi-interval modeling method for PV array based on working state analysis is proposed by adopting a refined seven-parameter model for PV cells [23]. PV array as the research object, photovoltaic module as the analysis unit, the equivalent circuit model and mathematical model of the module are combined. The different operating states of PV array are analysed and established a *I-U* mathematical model using the piecewise function method based on the output current characteristic equation.

The specific objectives of this study are to:

(1) Develop a comprehensive mathematical model for PV arrays under non-uniform illumination.

(2) Validate the model's accuracy under various shading patterns.

(3) Analyze the impact of different array configurations on power output.

(4) Provide guidelines for practical implementation.

2 THE PHOTOVOLTAIC ARRAY MODEL

2.1 Seven-Parameter Model for PV Cells

The refined seven-parameter (I_{pv}, I_{o1}, I_{o2}, A_1, A_2, R_s, and R_p) model of PV cells can better describe the light dark and high temperature characteristics, and is suitable for modelling PV arrays and studying output characteristics in multi-illumination environments [24]. The equivalent circuit model is shown in Fig. 1. The V-I mathematical model is as follows:

$$I = I_{pv} - I_{D1} - I_{D2} - I_p = I_{pv} - I_{o1}\left[\exp\left(\frac{V+IR_s}{A_1V_T}\right)-1\right] - I_{o2}\left[\exp\left(\frac{V+IR_s}{A_2V_T}\right)-1\right] - \frac{V+IR_s}{R_p} \tag{1}$$

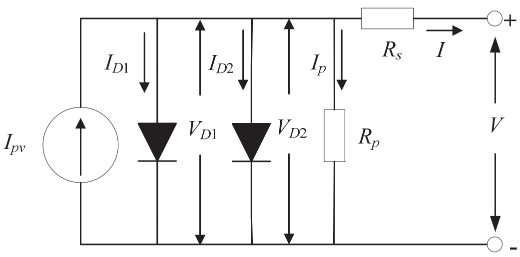

Figure 1 Seven-parameter equivalent circuit model

I: The output current, A
V: The output voltage, V
I_{pv}: Photogenerated current, A
q: Unit charge, 1.6022×10^{-19} C
K: Boltzmann constant, 1.3806×10^{-23} J/K
T: Absolute temperature, K
V_T: Thermal voltage, $V_T = KT/q$,V
R_s: Series resistor, Ω
R_p: Parallel resistor, Ω
I_{o1}, I_{o2}: D1, D2 response saturation current, A
A_1, A_2: Ideal factors for D1 and D2

2.2 Seven-Parameter Model of PV Cells

A PV module consists of n cells connected in series, with a series resistance R_{ms} and a parallel resistance R_{mp}:

$$\begin{cases} R_{ms} = nR_s \\ R_{mp} = nR_p \end{cases} \tag{2}$$

The module V-I mathematical model:

$$I = I_{pv} - I_o\left[\exp\left(\frac{V+nR_sI}{nV_T}\right)+\exp\left(\frac{V+nR_sI}{2nV_T}\right)-2\right] - \frac{V+nR_sI}{nR_p} \tag{3}$$

2.3 Equivalent Circuit Model of PV Array

2.2.1 Serial Array

The serial array structure composed of Ns modules is shown in Fig. 2. Illumination distribution of modules is: $G_1 > G_2 >, \ldots, > G_{Ns}$. Parallel bypass diodes are used to prevent module thermal spot effects under multi-illumination conditions. Series blocking diodes prevent current backflow and ensure that the array can operate normally in any lighting environment. The equivalent circuit diagram of the series array is shown in Fig. 3.

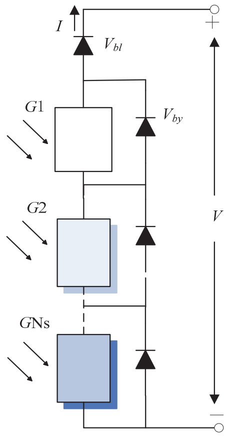

Figure 2 Series array

The photocurrents of each module are $I_{pv1}, I_{pv2}, \ldots, I_{pvNs}$ respectively. The output voltages are V_1, V_2, ..., V_{Ns} and the array current and voltage are I_s and V_s.

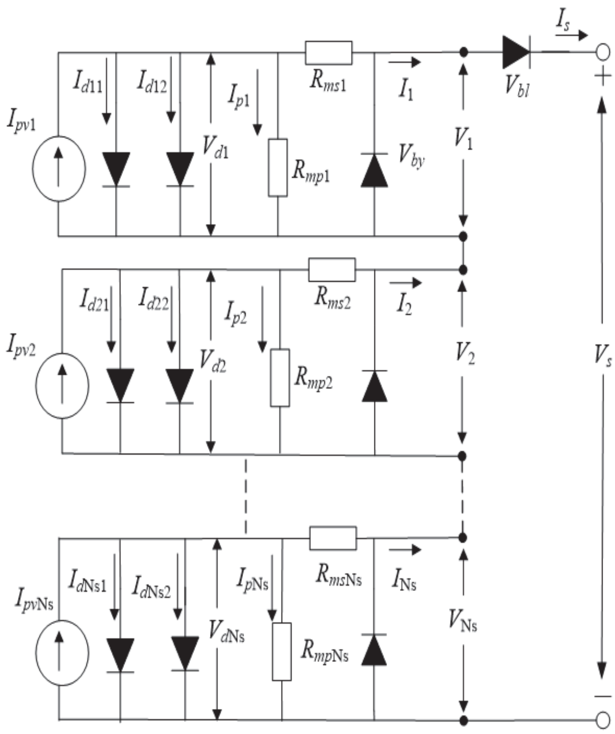

Figure 3 Equivalent circuit of series array

2.2.2 Parallel Array

The parallel array structure diagram composed of N_p modules is shown in Fig. 4 and the equivalent circuit in Fig. 5. The photocurrent of each module is I_{pv1}, I_{pv2}, …, I_{pvNp}, the output voltages are V_1, V_2, ..., V_{Np}, and the array current and voltage are I_p and V_p.

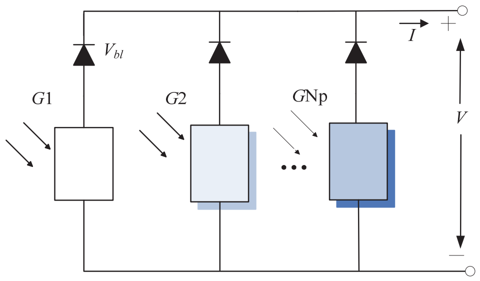

Figure 4 Parallel array

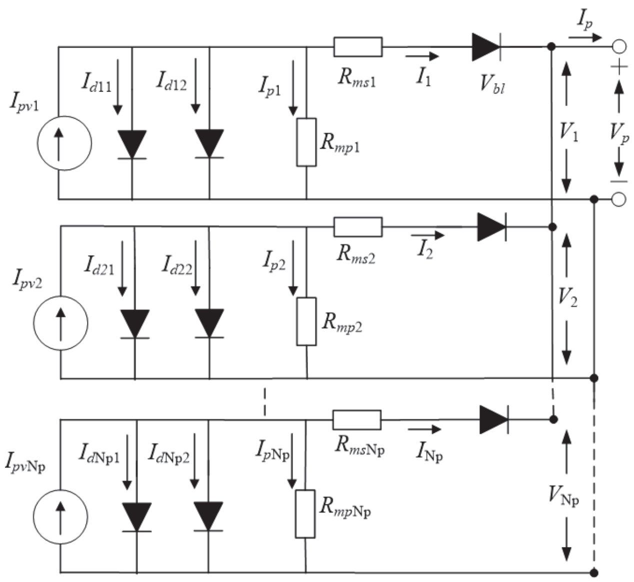

Figure 5 Equivalent circuit of parallel array

2.2.3 Series-Parallel Array

The $M \times N$ series-parallel array structure is shown in Fig. 6. The module illuminance is G_1, G_2, ..., G_N, and the photocurrent is I_{pv1}, I_{pv2}, …, I_{pvN}. The output voltages are V_1, V_2, ..., V_M, and the array currents and voltages are I_{sp} and V_{sp} respectively. The equivalent circuit of the $M \times N$ series parallel array is shown as Fig. 7.

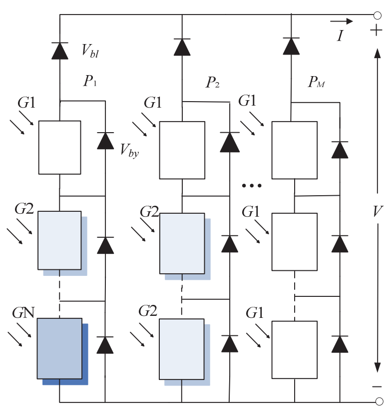

Figure 6 $M \times N$ series-parallel array

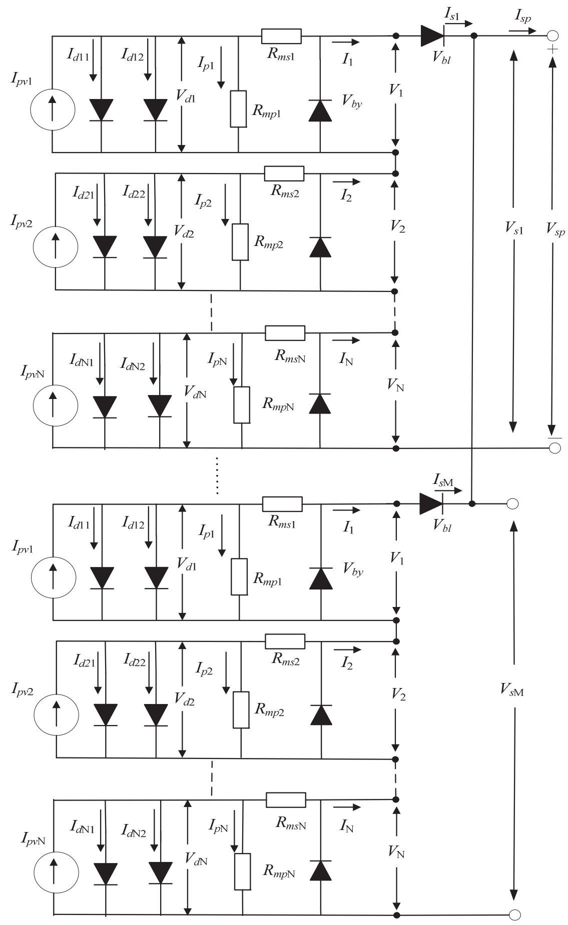

Figure 7 Equivalent circuit of $M \times N$ series-parallel array

3 MODELING THE WORK-STATUS OF PV ARRAYS

PV arrays with different topological structures exhibit complex nonlinearity in terms of current generation and output power under multi-level lighting. The circuit analysis method is used by the equivalent circuit model of the array. That is, the current of each module in series array is equal, and the voltage in parallel array is equal. In series-parallel array, the current of each series branch is equal, and the voltage of each parallel branch is equal. The battery model is divided into different current or voltage intervals, and operates in different states according to the illumination distribution. A segmented function model of the PV array is established to analyse the output characteristics.

3.1 Series Array Multi-Interval Current Analysis Method

N modules are connected in series, with an illuminance level of L. Assuming there are N_1 modules for illumination G_1, called substrings G_1 and N_L modules for illumination G_L, called substrings G_L. The photocurrent of each substring is I_{pv1}, I_{pv2}, …, I_{pvL}, short circuit current: I_{cs1}, I_{cs2}, …, I_{csL}, output voltages: V_{N1}, V_{N2}, ..., V_{NL}. The series resistance and parallel resistance of any substring i can be expressed as:

$$\begin{cases} R_{s\_zsi} = R_{ms} \mathrm{N}_i \\ R_{s\_zpi} = R_{mp} \mathrm{N}_i \end{cases} \quad (i = 1 \sim \mathrm{L}) \tag{4}$$

The corresponding substrings in each interval are analysed by dividing the array current into L intervals, and the analysis of the array under multi-illumination is transformed into a series of substrings under a single illumination. There are N_L working states, and two of them are analysed below:

Output power of N modules. N modules output power as $I \in [0, I_{scNL}]$. I_L of the substring G_L is: $I_L = I_s$, V_s is the sum of each substring V_{Ni}.

$$V_{Ni} = NiR_{s\_zpi}\left\{ I_{pvi} - I_o \left[\begin{array}{l} exp\left(\dfrac{V_{Ni} + R_{s\_zsi} I_s Ni}{V_{mT1} Ni} + \right) + \\ exp\left(\dfrac{V_{Ni} + R_{s\_zsi} I_s Ni}{2NiV_{mT2}}\right) - 2 \end{array} \right] - I_s \right\} - R_{s\_zsi} I_s Ni$$

$$V_s = \sum_{i=1}^{L} V_{Ni} + V_{bl} \tag{5}$$

$N_1, N_2, ..., N_{L-i}$ ($i = 1 \sim L - 1$) module output power. The substrings G_1, G_2, ..., G_{L-I} output power as $I \in [I_{sc(L-i)}, I_{sc(L-i-1)}]$. The bypass diodes conduct which connected parallel with substrings G_{L-i+1}, $G_{(L-i+2)}$,..., G_L. The currents are $I_s - I_{pv(L-i+1)}$, $I_s - I_{pv(L-i+2)}$,…, $I_s - I_{pvL}$, and the bypass diode voltages are $V_{by(L-i+1)}$, $V_{by(L-i+2)}$,…,V_{byL}. The output voltage of the array is:

$$\begin{aligned} V = {} & V_{N1} + V_{N2} +, \ ..., \ + V_{N(L-i)} + \\ & + N_{(L-i+1)} V_{by(L-i+1)} +, \ ..., \ + N_L V_{byL} + V_{bl} \end{aligned} \tag{6}$$

Output voltage of any substring G_j($j = 1 \sim L - i$):

$$\begin{aligned} V_{Nj} = {} & NjR_{zpj}\left\{ I_{pvj} - I_o \left[\begin{array}{l} \exp\left(\dfrac{V_{Nj} + R_{zsj} I_s Nj}{V_{mT1} Nj}\right) + \\ \exp\left(\dfrac{V_{Nj} + R_{zsj} I_s Nj}{2NjV_{mT2}}\right) - 2 \end{array} \right] - I_s \right\} - \\ & - R_{zsj} I_s Nj \end{aligned} \tag{7}$$

Based on Eq. (3) to Eq. (7), the mathematical model consists of L-segment functions in L intervals. Each interval corresponding to the distribution of local maximum power points is $P_{m1}(I_{m1}, V_{m1})$, $P_{m2}(I_{m2}, V_{m2})$,…, $P_{mN}(I_{mN}, V_{mN})$. The relationship between local maximum power point I_{mi} and open circuit I_{csi} satisfies the following equation:

$$\begin{cases} I_{m1} \approx C_I I_{sc1} \\ I_{m2} \approx C_I I_{sc2} \\ \vdots \\ I_{mN} \approx C_I I_{scN} \end{cases} \tag{8}$$

C_I: Short circuit current proportional coefficient, $0 < C_I < 1$

3.2 Parallel Array Multi-Interval Voltage Analysis Method

N_p modules are connected in parallel with an illuminance level of L. Assuming there are N_1 modules for G_1, called substrings G_1 and N_L modules for G_L, called substrings G_L. $N_p = N_1 + N_2 +, \ ..., \ + N_L$

PV current of each substring is $N_1 I_{pv1}$, $N_2 I_{pv2}$, …, $N_L I_{pvNp}$ open circuit voltage is V_{oc1}, V_{oc2}, …, V_{ocNp}, output current is I_1, I_2, …, I_L respectively. Series resistance and parallel resistance of any series are represented as:

$$\begin{cases} R_{p\_zsi} = R_{ms} / N_i \\ R_{p\_zpi} = R_{mp} / N_i \end{cases} \quad (i = 1 \sim L)$$

The output voltage is divided into L independent intervals, and the substrings in each interval are parallel arrays of single illuminance. Taking the substrings as the analysis object, there are N_L working states. The following two situations are analysed:

N_p module output power. When $U \in [0, V_{ocL}]$, N_p modules output power, substring G_L outputs voltage V_{NL}, current I_L, and array output voltage is determined by substring G_L. The V-I expression of G_L:

$$\begin{aligned} V_{NL} = {} & NLR_{p\_zpL}\left\{ I_{pvL} - I_o \left[\begin{array}{l} \exp\left(\dfrac{V_{NL} + R_{p\_zsL} I_L NL}{V_{mT1} NL}\right) + \\ \exp\left(\dfrac{V_{NL} + R_{p\_zsL} I_L NL}{2NLV_{mT2}}\right) - 2 \end{array} \right] - I_L \right\} - \\ & - R_{p\_zsL} I_L NL \end{aligned}$$

Parallel array output V_p and I_p:

$$\begin{cases} V_p = V_{NL} + V_{blL} \\ I_p = I_1 + I_2 + \cdots + I_L \end{cases} \tag{9}$$

$N_1, N_2, ..., N_{L-i}$, ($i = 1 \sim L - 1$) module output power. When the voltage $U \in [V_{oc(L-i-1)}, V_{oc(L-i)}]$, the substrings G_1, G_2, and G_{L-i} output power. Taking substrings G_{L-i} as the analysis object, output voltage is:

$$\begin{aligned} V_{N(L-i)} = {} & N(L-i) R_{p\_zp(L-i)}\left\{ I_{pv(L-i)} - I_o \left[\begin{array}{l} \exp\left(\dfrac{V_{N(L-i)} + R_{p\_zs(L-i)} I_{(L-i)} N(L-i)}{V_{mT1} N(L-i)}\right) + \\ + \exp\left(\dfrac{V_{N(L-i)} + R_{p\_zs(L-i)} I_{(L-i)} N(L-i)}{2N(L-i) V_{mT2}}\right) - 2 \end{array} \right] \right\} \\ & - R_{p\_zs(L-i)} I_{(L-i)} N(L-i) \end{aligned}$$

Parallel array output V_p and I_p:

$$\begin{cases} V_p = V_{N(L-i)} + V_{bl(L-i)} \\ I_p = I_1 + I_2 +, \ ..., \ + I_{(L-i)} \end{cases} \quad (i = 1 \sim L - 1) \tag{10}$$

Based on above analysis, the $I_p - V_p$ segmentation function model is as follows at L illumination levels:

$$\begin{cases} I_p = \sum\limits_{i=1}^{L} \left\{ \begin{array}{l} N_i I_{pvi} - N_i I_o \left[\exp\left(\dfrac{V_p - V_{bli} + R_{p\_zsi} I_i}{V_{mT}}\right) + \exp\left(\dfrac{V_p - V_{bli} + R_{p\_zsi} I_i}{2V_{mT}}\right) - 2 \right] \\ - \dfrac{(V_p - V_{bli}) + R_{p\_zsi} I_i}{R_{p\_zpi}} \qquad (0 \le V_p \le V_{ocL}) \end{array} \right\} \\ \vdots \\ I_p = \sum\limits_{i=1}^{L-j} \left\{ \begin{array}{l} N_i I_{pvi} - N_i I_o \left[\exp\left(\dfrac{V_p - V_{bli} + R_{p\_zsi} I_i}{V_{mT}}\right) + \exp\left(\dfrac{V_p - V_{bli} + R_{p-zsi} I_i}{2V_{mT}}\right) - 2 \right] \\ - \dfrac{(V_p - V_{bli}) + R_{p\_zsi} I_i}{R_{zpi}} \qquad \left(V_{oc(j+1)} < V_p \le V_{ocj} \right) j = 1 \sim L - 1 \end{array} \right\} \end{cases} \tag{11}$$

The array has a maximum power point P_m (I_m, V_m), as $U \in [0, V_{ocL}]$. The relationship of V_m and V_{oc} satisfies the following equation: $V_m \approx C_V V_{oc}$

C_V: proportional coefficient of open circuit voltage, $0 < C_V < 1$.

3.3 Serial-Parallel Array Multi-Interval Voltage and Current Analysis Method

Assuming that M × N series-parallel array has L illumination levels, $G_1 > G_2 >, ..., > G_L$ .In M_1 branch, there are N_{11} modules with illumination G_1, denoted as N_{11} (G_1), and so on. The module with illumination G_L is denoted as N_{1L} (G_L), $L = 1 \sim N$. $N_{11} + N_{12} + N_{13} +, ..., + N_{1L} = N$. The illumination distribution in the M branch is $N_{M1}(G_1)$, $N_{M2}(G_2)$, …, $N_{ML}(G_L)$, and $N_{M1} + N_{M2} +, ..., + N_{ML} = N$ .Based on voltage, the operating voltage of the array is divided into M intervals: $[0 , N_{11}V_{oc1} + N_{12}V_{oc2} + L + N_{1L}V_{ocL}]$, $(N_{11}V_{oc1} + N_{12}V_{oc2} +, ..., + N_{1L}V_{ocL}, N_{21}V_{oc1} + N_{22}V_{oc2} +, ..., + N_{2L}V_{ocL}]$, $\left[N_{(M-1)1}V_{oc1} + N_{(M-1)2}V_{oc2} +, ..., + N_{(M-1)(L-1)}V_{oc(L-1)}\right.$,$\left[\right.$ $N_{M1}V_{oc1} + N_{M2}V_{oc2} +, ..., + N_{ML}V_{ocL}]$.

3.3.1 M Branches Output Power

As $U \in [0, N_{11}V_{oc1} + N_{12}V_{oc2} +, ..., + N_{1L}V_{ocL}]$, M branches output power. The V and I can be expressed as:

$$\begin{cases} V = V_i + V_{bli} \\ I = \sum_{i=1}^{m} I_i \end{cases} \tag{12}$$

V_i, I_i: output voltage and current of the i ($i = 1 \sim m$) branch.

The I branch. The L illuminance levels G_1, G_2, ..., G_L in the I branch divide the current into L intervals: [0, I_{csL}], ($I_{cs(L-1)}$, I_{csL}], …, (I_{cs2}, I_{cs1}]. Segmented function expression is:

$$\begin{cases} V = N_{11}V_{11} + N_{12}V_{12} +, ..., + N_{1L}V_{1L} + V_{bl1} & \left(0 \le I_1 \le I_{csL}\right) \\ V = N_{11}V_{11} + N_{12}V_{12} +, ..., + N_{1(L-1)}V_{1(L-1)} & \\ +V_{bl1} + N_{1L}V_{by} & \left(I_{csL} < I_1 \le I_{cs(L-1)}\right) \\ \vdots & \\ V = N_{11}V_{11} + V_{bl1} + \left(N_{12} + N_{13} +, ..., + N_{1L}\right)V_{by} & \left(I_{cs2} < I_1 \le I_{cs1}\right) \end{cases} \tag{13}$$

V_{1i}: N_{1i} (G_i) ($i = 1 \sim L$) module output voltage:

$$V_{1i} = R_{mp}\left\{ I_{pvi} - I_o \left[\begin{aligned} &\exp\left(\frac{V_{1i} + R_{ms}I_1}{V_{T1}}\right) + \\ &+\exp\left(\frac{V_{1i} + R_{ms}I_1}{2V_{T2}}\right) - 2 \end{aligned} \right] - I_1 \right\} - R_{ms}I_1 \tag{14}$$

$$\left(i = 1, 2, ..., L\right)$$

By analogy, the segmented function expressions for branches II, III, ..., ($M - 1$) can be obtained.

The M branch. The voltage of branch M is equal to the voltage of branches I, II, ..., ($M - 1$). The illumination level of branch M is L_m, current I_m, V and I can be expressed as: $V = N_{m1}V_{m1} + N_{m2}V_{m2} +, ..., + N_{mLm}V_{mLm} + V_{blm}$.

The voltage intervals of array determine whether each branch works. As $U \in \left[N_{11}V_{oc1} + N_{12}V_{oc2} +, ..., + N_{1L}V_{ocL}\right.$, $\left. N_{21}V_{oc1} + N_{22}V_{oc2} +, ..., +N_{2L}V_{ocL}\right]$, if the output voltage of branch I is less than this range voltage, no power output. Similarly, as the voltage range gradually increases, branches II, III, ..., ($M - 1$) do not output power.

3.3.2 The *M*-th Branch Output Power

As $U \subset \left(N_{(M-1)1}V_{oc1} + N_{(M-1)2}V_{oc2} +, ..., + N_{(M-1)(L-1)}V_{oc(L-1)}\right.$, $\left. N_{M1}V_{oc1} + N_{M2}V_{oc2} +, ..., + N_{ML}V_{ocL}\right]$ the M-th branch output power, L illuminance divides the current into L intervals: [0, I_{csL}], (I_{csL}, $I_{cs(L-1)}$], …, (I_{cs2}, I_{cs1}]. The segmented function is as follows:

$$\begin{cases} V = N_{M1}V_{M1} + N_{M2}V_{M2} +, ..., + N_{ML}V_{ML} + V_{blM} & \left(0 \le I_m \le I_{csL}\right)] \\ V = N_{M1}V_{M1} + N_{M2}V_{M2} +, ..., + N_{M(L-1)}V_{M(L-1)} + V_{blM} + N_{MLM}V_{by} & \\ \left(I_{csL} < I_m \le I_{cs(L-1)}\right)] & \\ \vdots & \\ V = N_{M1}V_{M1} + V_{blM} + (N_{M2} + N_{M3} + L + N_{ML})V_{by} & \left(I_{cs2} < I_m \le I_{cs1}\right)] \end{cases} \tag{15}$$

V_{Mi}: theN_{Mi} (G_i) ($i = 1 \sim L$) module output voltage.

The maximum power point is determined by the illumination distribution of I branch when the array outputs power, and the distribution of power points in each current interval satisfies Eq. (8).

From above, any illumination level and array structure can be used to establish a segmented function model by the multi- interval work-state analysis method.

4 EXPERIMENT, RESULTS AND DISCUSSION

4.1 Experimental Environment Setup

Simulation and data acquisition experiments are conducted by using series array of 3 modules, parallel array of 3 modules, and series-parallel array of 3 × 3 modules under T = 25 °C, AM1.5, G_1 = 1000 W/m^2, G_2 = 600 W/m^2, G_3 = 300 W/m^2. Based on the segmented function model, a simulation model of the array is established by MATLAB programming and the theoretical curve is obtained by the numerical solution. The output characteristics correctness of the model is verified by comparing simulation and experimental data, and the error analysis is conducted under multi-illumination. The photovoltaic array experimental system is built to obtain data by a microcontroller data acquisition system in the laboratory. The current and voltage values are measured by changing the environmental temperature, illumination, and array topology. The maximum power value calculated is compared with simulation data to analyse the error. The electrical parameters of the refined seven-parameter model are shown in Tab. 1 for Kyocera's KG200GT. The experimental simulation process is shown in Fig. 8.

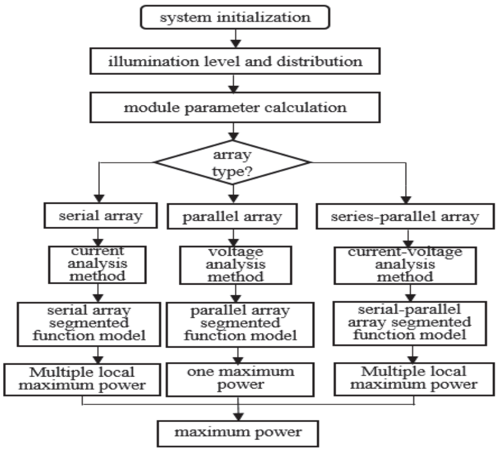

Figure 8 The experimental simulation process

Table 1 Electrical parameters of refined seven-parameter model for Kyocera's KG200GT

Battery structure	N batteries in series, $n = 54$
Maximum power P_m	200 W
Maximum power point voltage V_m	26.3 V
Maximum power point current I_m	7.61 A
Reverse saturation current of diode I_o	4.128 × 10−10 A
Photogenerated currentI_{pv}	4.73 A
Series resistor R_s	0.335 Ω
Parallel resistor R_p	155.48 Ω

4.2 Array Simulation and Experimental Output Characteristic Analysis

4.2.1 Serial Array Simulation And Experiment

The illumination levels of the three series modules are G_1, G_2, and G_3, respectively. The array structure and illumination distribution are shown in Tab. 2. The simulation and experimental output characteristic curves *V-I* and *V-P* are shown in Fig. 9 and Fig. 10.: experimental data

Curve I. The pink curve serves as a reference under standard conditions, with a maximum power point at G_1 illumination: P_m = 602.8759 W.

Table 2 Illumination distribution of three series modules (T = 25 °C, AM1.5)

Type	Total modules	G_1 / W/m² 1000	G_2 / W/m² 600	G_3 / W/m² 300
I	3	3	0	0
II	3	1	1	1
III	3	2	1	1
IV	3	1	2	0

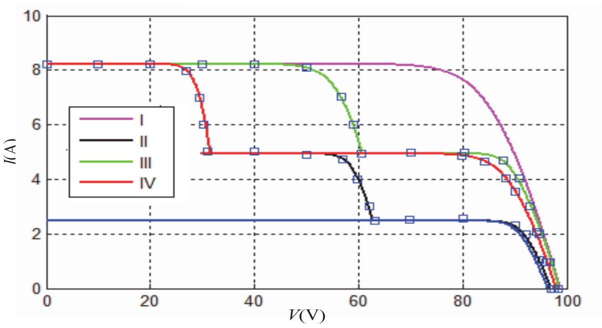

Figure 9 Simulation and experimental curves for *V-I* of series array under multi-illumination

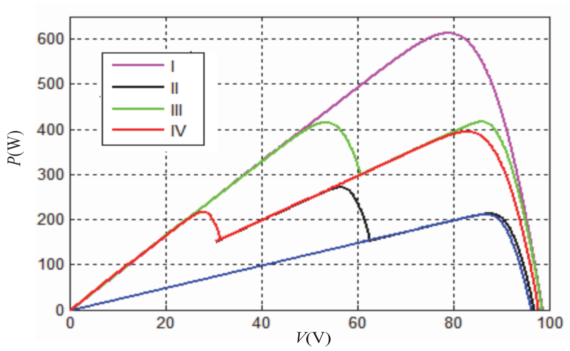

Figure 10 Simulation curves for *V-P*of series array under multi-illumination

Curve II. It consists of three black curves on three current intervals [0, I_{cs3}], (I_{cs3}, I_{cs2}], (I_{cs2}, I_{cs1}] determined by three illuminance levels, each interval having a local maximum power. They are respectively P_{m1} = 212.4625 W, P_{m1}(88.3641 V, 2.4044 A), P_{m2} = 271.0544 W, P_{m2}(56.7972 V, 4.7723 A), P_{m3} = 216.7306 W, P_{m3}(28.2258 V, 7.6785 A). The distribution of maximum power point current I_{mi} satisfies Eq. (8). The *I-V* curve has three knee points, and the current value decreases in a stepped manner, corresponding to the working states of one module, two modules, and three modules in terms of external output power. From the local maximum power values of each interval, it can be seen that the local P_m is not only related to the current interval, but also to the number of modules that jointly output power.

Curve III. It consists of two green curves in the current interval [0, I_{cs2}] and (I_{cs2}, I_{cs1}] with two levels of illumination and corresponding two local maximum power points: P_{m1} = 416.2562 W, P_{m1}(86.2903 V, 4.8239 A), P_{m2} = 414.7946 W, P_{m2}(53.8018 V, 7.7096 A). The *I-V* curve has two knee points, corresponding to the output power of one module and three modules respectively.

Curve IV. It is red curve as the same illumination as III, but different distributions. The values of local maximum power are P_{m1} = 394.3506 W, P_{m1}(82.8341 V, 4.7607 A), P_{m2} = 216.7306 W, P_{m2}(28.2258 V, 7.6785 A). Its local maximum power value and global maximum power value are both lower than type III. Therefore, the illumination distribution directly affects the value of maximum power output.

The blue curve.It represents the output characteristic curve of modules in the array without parallel bypass diodes. Bypass diodes can not only protect the battery from hot spot effects, but also increase the output power. The *V-I* curve drawn from the experimental data is basically consistent with the simulation curve data, which verifies the correctness and accuracy of the segmented function model under multi-illumination conditions, as well as the theoretical analysis of the series array.

4.2.2 Parallel Array Simulation and Experiment

The illumination of parallel module is G_1, G_2, G_3, and the illumination distribution of the three modules is shown in Tab. 3 for types I, II, III, and IV. The simulation and experimental curves of *V-I* and *V-P* in parallel array are shown in Fig. 11 and Fig. 12.

Table 3 Illumination distribution of three parallel modules (T = 25 °C, AM1.5)

Type	Total modules	G_1 / W/m² 1000	G_2 / W/m² 600	G_3 / W/m² 300
I	3	3	0	0
II	3	1	1	1
III	3	2	1	0
IV	3	1	2	0

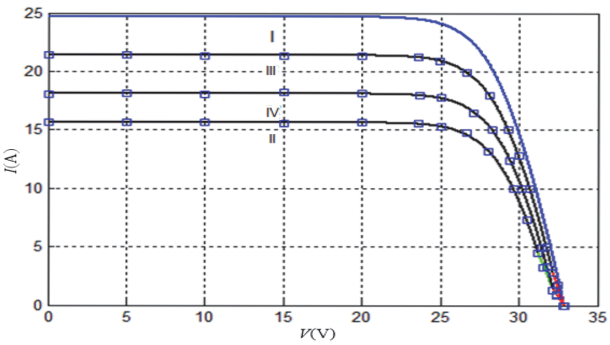

Figure 11 Simulation and experimental curves for *V-I* of parallel array under multi-illumination

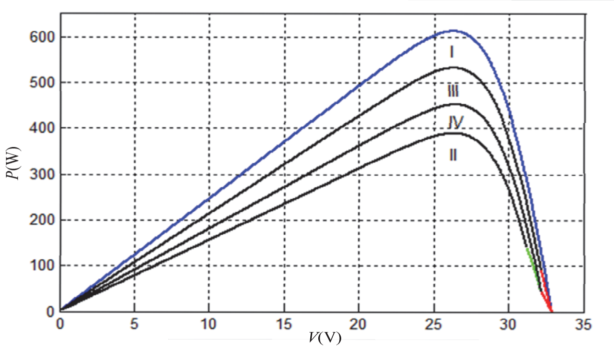

Figure 12 Simulation curves for *V-P* of parallel array under multi-illumination

The unimodal characteristic curve of parallel array under multi-illumination is roughly the same as that of single illumination. The global maximum power point is located within the minimum illumination interval on the first curve, and all modules output power within this interval. The power and current values are the sum of outputs of all parallel modules, The relationship of V_m and V_{oc} satisfies the equation: V_m = (0.8 - 1) V_{oc}. In other intervals, as the voltage value increases, P and I rapidly decrease to 0. Compared to a single illumination, the power significantly decreases under multi-illumination conditions, mainly due to the significant influence of G on I_{pv}, which verifies the correctness of the parallel array theory analysis and mathematical model.

4.2.3 Series-Parallel Array Simulation and Experiment

The light distribution of the 3 × 3 array is shown in Tab. 4. The *V-I* and *V-P* simulation and experimental output characteristic curves are shown in Fig. 13 and Fig. 14.

Table 4 Illumination distribution of nine series-parallel modules (T=25℃,AM1.5)

Type	Total modules	G_1 / W/m² 1000	G_2 / W/m² 600	G_3 / W/m 300
P1	3	1	1	1
P2	3	0	3	0
P3	3	3	0	0

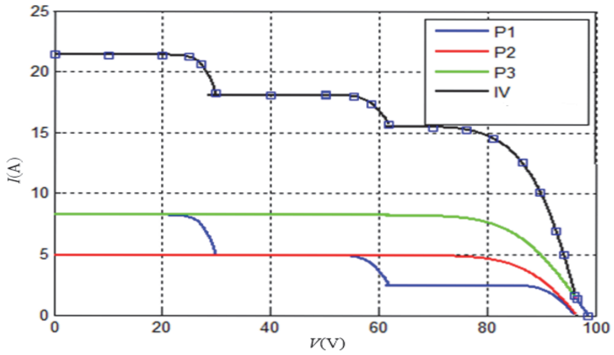

Figure 13 Simulation and experimental curves for *V-I* of 3×3 series-parallel array under multi-illumination

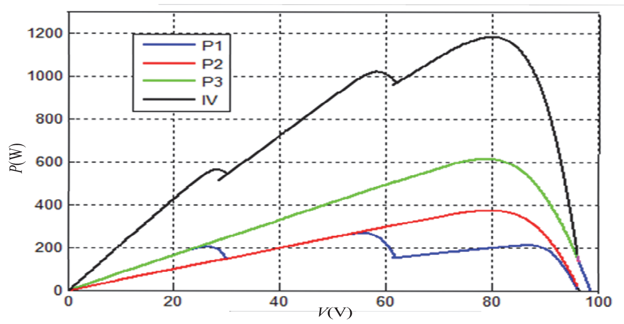

Figure 14 Simulation curves for *V-P* of 3 × 3 series-parallel array under multi-illumination

According to the illumination distribution of the array in Tab. 4, the voltage range is divided into three intervals: [0, $V_{oc3} + V_{oc2} + V_{oc1}$]，($V_{oc3} + V_{oc2} + V_{oc1}$, 3$V_{oc2}$]，(3$V_{oc2}$, 3$V_{oc1}$].

As U∈ [0, $V_{oc3} + V_{oc2} + V_{oc1}$], all modules in the array output power. The three current intervals [0, I_{cs3}], (I_{cs3}, I_{cs2}], (I_{cs2}, I_{cs1}] of P1 branch are composed of three blue curves with three local maximum power points. Both P2 and P3 branches have red and green unimodal curves with one illuminance. Curve IV is the physical superposition of three curves, and the local power value is determined by the current interval of P1 branch. The relationship between I_m and I_{cs} satisfies the equation: $I_m \approx C_I I_{sc}$

C_I: the proportional coefficient of short-circuit current, $0 < C_I < 1$.

As U∈(V_{oc3}+V_{oc2}+V_{oc1}, 3V_{oc2}], P1 branch does not output power due to the blocking diode being turned off. P1 branch has no output in this interval P2, P3, and IV correspond to black, red, and magenta curves respectively.

As U∈(3V_{oc2}, 3V_{oc1}], only P3 branch outputs power and P3 branch and IV output are equal. The curves coincide in this interval, represented by the blue curve.

The entire array output IV consists of 5 curves, among which 3 output voltage intervals determine 3 curves with 3 inflection points, which are the endpoints of the voltage intervals. The open circuit voltage of the array is determined by the maximum illumination, V_{oc} = 3V_{oc1}. The maximum power point is located in the first voltage range, and the three local maximum power points are P_{m11} = 563.0375 W, P_{m11}(28.0246 V, 20.0908 A), P_{m12} = 1018.8031 W, P_{m12}(58.3648 V, 17.4558 A), P_{m13} = 1181.4217 W, P_{m13}(80.3875 V, 14.6966 A). The voltage range of the branch is [0, V_{oc3}], (V_{oc3}， $V_{oc2} + V_{oc1}$], ($V_{oc2} + V_{oc1}$, $V_{oc3} + V_{oc2} + V_{oc1}$], still satisfies with the relationship V_m = (0.8 ～ 1)V_{oc}. Curve IV is the superposition of the outputs from branches P1, P2, and P3, which exhibit series characteristics within a certain current range and have a shape similar to curve P1. It exhibits parallel characteristics within a certain voltage range, verifying the correctness of the theoretical analysis of series-parallel arrays.

According to the distribution of maximum power points, the array structure and illuminance distribution directly affect the maximum output power and output curve shape. When the illumination and distribution are the same, the power output of parallel array exhibits a unimodal characteristic, making it easier to track the maximum power point compared to series array. When the illumination of each parallel branch of the series-parallel array is the same, the array can maximize the output power. The output characteristics are close to the unimodal characteristics under a single illumination, which makes it easier to track and control the maximum power point. It provides a mathematical model for photovoltaic array configuration and the research of maximum power point tracking algorithm under complex illumination.

4.3 Experimental Error Analysis

The maximum power point values obtained from the experimental measured and simulation data of photovoltaic arrays based on work-state analysis method are shown in the Tab. 5, Tab. 6 and Tab. 7. Through error analysis, it can be concluded that the maximum measurement and simulation error for any photovoltaic array structure is less than 1.5%. While existing models provide reasonable accuracy under uniform illumination, they fail to capture complex behaviors under partial shading conditions, leading to significant power prediction errors (typically 15 - 20%). Segmented function modeling method is comparable to the accuracy of machine learning algorithms, but its computational complexity is significantly lower than that of machine learning, ensuring both computational speed and accuracy.

Table 5 Analysis of maximum power error in series array

Type	Simulation data	Measurement data	relative error
I	602.8759W	598.4125	0.74%
II	271.0544W	275.1045	1.47%
III	416.2562W	419.3384	0.73%
IV	394.3506W	398.1175	0.95%

Table 6 Analysis of maximum power error in parallel array

Type	Simulation data	Measurement data	relative error
I	602.8759W	608.1154	0.86%
II	394.0026W	390.0221	1.02%
III	532.6255W	528.9947	0.69%
IV	456.4565W	460.6601	0.91%

Table 7 Analysis of maximum power error in series-parallel array

Type	Simulation data	Measurement data	relative error
P1	563.0375W	569.2445	1.09%
P2	1018.8031W	1009.7012	0.90%
P3	1181.4217W	1196.9736	1.30%

5 CONCLUSION

This paper presents a novel work-state analysis method for modeling PV array under complex illumination conditions, which can be used for arrays sizes and illumination levels of any topology structure. It solves the modeling problem of photovoltaic array and provides a theoretical basis for the configuration and maximum power point tracking of photovoltaic array. The key findings include:

(1) The proposed segmented function model accurately predicts array behavior under multiple illumination levels, with validation errors below 1.5%.

(2) Series array exhibits multiple maximum power points, with positions predictable using the developed mathematical framework.

(3) Parallel configurations demonstrate unified characteristics, simplifying maximum power point tracking.

(4) The model successfully captures the hybrid characteristics of series-parallel arrangements. The practical implications include improved design optimization capabilities and enhanced maximum power point tracking efficiency. Future work should focus on real-time implementation and integration with smart grid applications.

Acknowledgements

This paper is supported by Humanities and Social Sciences Planning Fund of the Ministry of Education (22YJA630111) and Beijing Key Laboratory of Intelligent Processing for Building Big Data.

6 REFERENCES

[1] Wang, C. & Zhang, X. (2023). A survey of output characteristics and power optimization technology of photovoltaic array in mismatch scenario. *The 5th International Conference on Power and Energy Technology*, Guangzhou, China, 1491-1495. https://doi.org/10.1109/ICPET59380.2023.10367536

[2] Lu, H., Shi, L., Yang, H. X., et al. (2017). Simulation analysis of influence of shadow occlusion on power generation capacity of solar array. *Spacecraft Environmental Engineering*, *34*(03), 252-257.

[3] Stein, J. S. (2017). PV performance modelingmethodsand practices. *Results from the 4th PV Performance Modeling Collaborative Workshop*. https://doi.org/10.2172/1347082

[4] Gao, Y., Wu, D., Dai, Z., Changling, W., Bo, C., & Xiaosong, Z. (2023). A comprehensive review of the current status, developments, and outlooks of heat pipe photovoltaic and photovoltaic/thermal systems. *Renewable Energy*, *207*, 539-574. https://doi.org/10.1016/j.renene.2023.03.039

[5] Zhu, H., Cao, Y., Lu, L., Weiwei, L., Jianxi, Y., & Yang, H. (2018). Research on parameter distribution features of photovoltaic array under the cover and shadow shading conditions. *International Journal of Photoenergy*, 1-14. https://doi.org/10.1155/2018/9207917

[6] Yao, Y., Wang, Y., Jia, H., & Yunfei, M. (2023). An analytical approach based on coupled multi-physics model forphotovoltaic arrays performance simulation. *Electric Power Systems Research*, *224*, 1-16. https://doi.org/10.1016/j.epsr.2023.109773

[7] Orozco-Gutierrez, M. L., Ramirez-Scarpetta, J. M., Spagnuolo, G., & Ramos-Paja, C. A. (2014).Amethod for simulating large PV arrays that include reverse biased cells. *Applied Energy*, *123*, 157-167. https://doi.org/10.1016/j.apenergy.2014.02.052

[8] Fu, R., Li, G., Shi, J., & Zhaoyu, J. (2022). Research on the model of photovoltaic array output electrical characteristics

based on the multi-inclination condition. *2022 34th Chinese Control and Decision Conference*, 821-826. https://doi.org/10.1109/CCDC55256.2022.10033668

[9] Sun, Y., Hou, J., & Li, R. (2014). Photovoltaic array model and its solving algorithm based on hidden complementarity problem. *Chinese Journal of Electrical Engineering*, *34*, 6066-6073.

[10] Pachauri, R., Mahela, O., & Sharma, A. (2020).Impact of partial shading on various PV array configurations and different modelingapproaches: A comprehensive review. *IEEE Access*, *8*, 181375-181403. https://doi.org/10.1109/ACCESS.2020.3028473

[11] Chepp, E., Gasparin, F., & Krenzinger, A. (2022). Improvements in methods for analysis of partially shaded PV modules. *Renewable Energy*, *200*, 900-910. https://doi.org/10.1016/j.renene.2022.10.035

[12] Xia, S., Xu, J., & Guo, L. (2024).Real-time modelingmethod for large-scale photovoltaic power stations using nested fast and simultaneous solution. *IEEE Transactions Industrial Electronics*, 1-11. https://doi.org/10.1109/TIE.2024.3440469

[13] Olayiwola, T. & Choi, S. (2023). Superellipse model: An accurate and easy-to-fit empirical model for photovoltaic panels. *Solar Energy*, *262*, 11749. https://doi.org/10.1016/j.solener.2023.05.026

[14] Abdulmawjood, K., Alsadi, S., Refaat, S., & Morsi, W. (2022). Characteristic study of solar photovoltaic array under different partial shading conditions. *IEEE Access*, *10*, 6856-6866. https://doi.org/10.1109/ACCESS.2022.3142168

[15] Sharma, M., Pareek, S., & Singh, K. (2023). Robust reconfiguration strategies for maximum output power from large-scale photovoltaic arrays under partial shading conditions. *PhysicaScripta*, *98*(03), 035215. https://doi.org/10.1088/1402-4896/acb112

[16] Piccoli, E., Dama, A., Dolara, A., & Leva, S. (2019). Experimental validation of a model for PV systems under partial shading for building integrated applications. *Solar Energy*, *183*, 356-370. https://doi.org/10.1016/j.solener.2019.03.015

[17] Belghiti, H., Kandoussi, K., & Chellakhi, A. (2024). Performance optimization of photovoltaic system under real climatic conditions using a novel MPPT approach. *Energy Sources Part A-recovery Utilization and Environmental Effects*, *46*(01), 2474-2492. https://doi.org/10.1080/15567036.2024.2308656

[18] Zhang, J., Wei, X., Hu, L., Jian-Guang, Ma (2019). A MPPT method based on improved Fibonacci search photovoltaic array. *Tehnicki Vjesnik-Technical Gazette*, *26*(01), 163-170. https://doi.org/10.17559/TV-20180721153103

[19] Zhang, H., Wang, X., & Zhang, J. (2024).MPPT control of photovoltaic array based on improved marine predator algorithm under complex solar irradiance conditions. *Scientific Reports*, *14*(1), 19745. https://doi.org/10.1038/s41598-024-70811-x

[20] Ali, K., Khan, L., & Khan, Q. (2021). Neurofuzzy robust backstepping based MPPT control for photovoltaic system. *Turkish Journal of Electrical Engineering and Computer Sciences*, *29*, 421-436. https://doi.org/10.3906/elk-1907-15

[21] Teng, J., Wu, H., & Wu, Z. (2023). Efficient partial shading detection for photovoltaic generation systems. *IEEE Transactions on Sustainable Energy*, *14*(04), 2249-2259. https://doi.org/10.1109/TSTE.2023.3271298

[22] Phan, B., Lai, Y., & Lin, C. (2020). A deep reinforcement learning-based MPPT control for PV systems under partial shading condition. *Sensors*, *20*(11), 3039. https://doi.org/10.3390/s20113039

[23] Tifidat, K., Maouhoub, N., Salah, F., Askarb, S. S., & Mohamed, A. (2024). An adaptable method for efficient modelingof photovoltaic generators' performance based on the double-diode model. *Heliyon*, *10*(13), 1-18. https://doi.org/10.1016/j.heliyon.2024.e33946

[24] Tifidat, K., Maouhoub, N., Benahmida, A., & Fatima, E. A. S. (2022). An accurate approach for modeling I-V characteristics of photovoltaic generators based on the two-diode model. *Energy Conversion and Management*, *14*, 100205. https://doi.org/10.1016/j.ecmx.2022.100205

Contact information:

Jun-Hong ZHANG, Associate Professor, PhD, Department Head
(Corresponding author)
School of Electrical and information Engineering,
Beijing University of Civil Engineering and Architecture,
Beijing, 100044, China
E-mail: zhangjunhong@bucea.edu.cn

Ling-Yu LI, Master's students
School of Electrical and information Engineering,
Beijing University of Civil Engineering and Architecture
Beijing, 100044, China
E-mail: lilingyu0802@126.com

Chao-Yu ZHAI, undergraduate
College of Artificial Intelligence,
China University of Petroleum (Beijing)
Beijing, 102249, China
E-mail: zhaichaoyu2005@qq.com